Entangling Photons via Four-Wave Mixing in a Rubidium Vapor Cell

Kelly Roman

Advisor: I. Novikova

Quantum Optics Group, The College of William and Mary, Williamsburg

April 3, 2015

Abstract

We investigate electromagnetically induced transparency (EIT) and four-wave mixing (FWM) as mechanisms to generate entangled optical fields. Entanglement is a central concept of quantum mechanics, and holds promise for a variety of applications, including the realization of quantum cryptography and quantum teleportation. To achieve entangled optical fields, a strong control beam and a co-propagating orthogonally-polarized weak probe beam interact with Rb atoms inside a heated vapor cell. As a result of this interaction, the probe beam was amplified and a new Stokes field was generated under FWM conditions. We observed strong modification of EIT and FWM feature lineshapes with laser power and frequency variation. For evidence of optical field entanglement, we measured intensity and noise correlations between the probe and Stokes signals.

FWM is more effective with atomic quantum states of longer lifetimes. Unfortunately, when Rb atoms collide with the walls of the cell, their quantum state is destroyed. To circumvent this problem, paraffin coating is applied to the cell walls to reduce surface relaxation and allow atoms to maintain their quantum state upon collisions, thus increasing their lifetimes. In general, paraffin coating is known to create narrow resonances. To enhance any EIT and FWM features caused by the paraffin, a strong beam was sent co-propagating through the Rb cell with a weak beam in spatially separated regions. However, we found that in separated-regions EIT measurements, the observed narrow structure was identical to that observed in an uncoated cell, demonstrating that the coating had no clear effect on EIT or FWM.

Contents

1   Theory

1.1   Quantum Entanglement

The phenomenon of entanglement arises from the quantum mechanical treatment of the universe, and has fascinated public and scientific minds since its intriguing role in Einstein, Podolsky, and Rosen's thought experiment in 1935 [1]. The quantum state of a system can be described by its wavefunction, $\Psi(x,t)$, which is a function that holds the entirety of information about said system. For the physical implication of such a function, take the following wavefunction of a single particle:

$$P_{a \leq x \leq b}(t) = \int_a^b |\Psi(x,t)|^2 \, \mathrm{d}x. \tag{1}$$

Integrating over the square modulus of the wavefunction, equation 1 gives the probability of finding the particle at a position x between the points a and b. Entanglement occurs when two systems cannot be described by independent wavefunctions. Instead, some property of their quantum state is described by a linear superposition of available eigenstates [2] and they are "entangled". As a simple demonstration, take each system to consist of a single particle. It is possible to know that the combined spin of the two particles must equal zero ($s = 0$), but impossible to know which particle has spin $s = +1$ and which particle has spin $s = -1$. Thus, the wavefunction is written as a superposition of the two states, meaning that physically, the particles exist in both the $+1$ and -1 spin states at the same time. Upon measurement of one particle, the wavefunction collapses and an exact spin valued (e.g. $s = +1$) can be extracted. Simultaneously, the second particle, irregardless of spatial distance, 'knows' that a measurement has been made on the other particle and will take on the corresponding spin value (-1). The correlation between systems is characteristic of entanglement. Entanglement has promising implications for quantum teleportation, quantum cryptography, and quantum computing, among others.

1.2   Light Interaction with Atoms

Light most prominently interacts with matter through the absorption or emission of photons. If an atom absorbs a photon that has enough energy to span the gap between energy levels, an electron can be excited to a different quantum state. Similarly, an electron can be deexcited to a lower energy level if the atom emits a photon of a certain energy, given by:

$$\Delta E = h\nu \tag{2}$$

where h is Planck's constant and ν is frequency of the photon. The energy of the photon, or change in energy, is representative of the energy gap between atomic levels. In alkali atoms, like rubidium (Rb), there is a single valence electron which allows the spin to be optically aligned, and facilitates the coherence of resonant properties rather than the natural, but undesired process of spontaneous or incoherent emission.

Two non-linear optical processes were of particular interest in the search for entangled photons. Electromagnetically induced transparency (EIT) and four-wave mixing (FWM) both arise from coherent light interaction with atoms. Ultimately, FWM was used to produce entangled electric fields. However, EIT is a more prominent effect than FWM, so was analyzed and optimized first since both processes occur under similar conditions.

1.2.1   Electromagnetically Induced Transparency

Due to hyperfine splitting in alkali atoms, a separation of ground states occurs. Two coherent electric fields are tuned to resonance of the atomic transitions. The $5S_{1/2} \rightarrow 5P_{1/2}$ transitions in ^{87}Rubidium D1 line are the relevant transitions considered in this report.

(a) Relevant energy levels   (b) Corresponding absorption spectrum
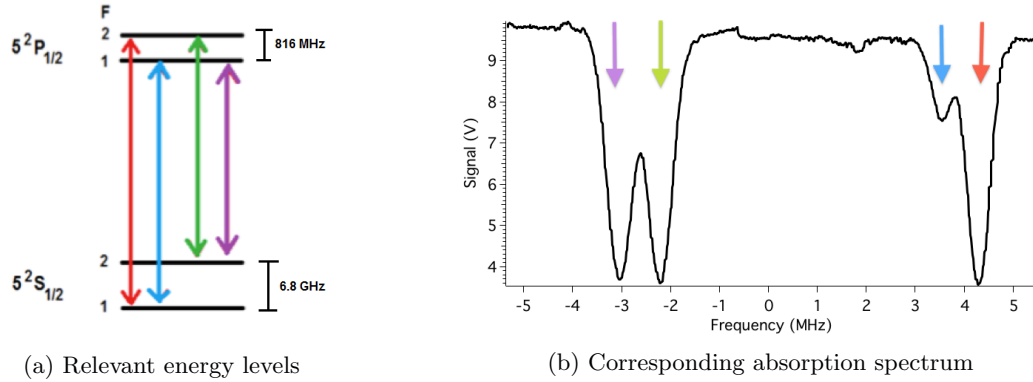
Figure 1: ^{87}Rb D1 line

For our purposes, we consider a three level Λ system (figure 2). One strong, control, field is tuned to the transition between one ground state $|g_2\rangle$ and a shared excited state $|e\rangle$, while the second, weak probe, field is tuned to the transition between the other degenerate ground state $|g_1\rangle$ and the excited state. From this configuration, atoms can be pumped to one of two states, which are a superposition of the two atomic ground states [3]:

$$|B\rangle = \frac{E_p |g_1\rangle + E_c |g_2\rangle}{\sqrt{E_p^2 + E_c^2}} \qquad (3) \qquad |D\rangle = \frac{E_c |g_1\rangle - E_p |g_2\rangle}{\sqrt{E_p^2 + E_c^2}} \qquad (4)$$

The bright (eq. 3) and dark (eq. 4) states are linear superpositions of the two ground states.

The effect of coherence on material becomes apparent as the atomic population in the $|D\rangle$ state increases (equation 4). Under resonant conditions, destructive interference occurs between the transition pathways in this state, and the atoms become non-interacting with the light. The inability for these atom populations to 'see' light characterizes the dark $|D\rangle$ state. As a result, probe beam photons view the material as transparent, and the probe beam passes through the atoms without any, or very little, absorption. Figure 3 shows the absorption of the electric field as a function of probe detuning from resonance, obtained from the imaginary part of the electric susceptibility (the degree of polarization the electric field experiences in Rb).
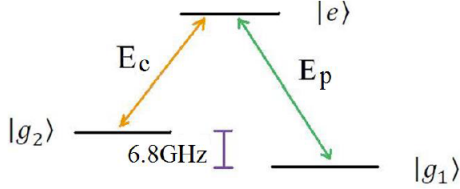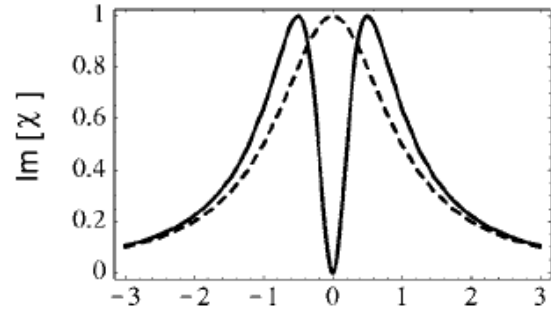
Figure 2: EIT Λ system

Figure 3: Imaginary part of the susceptibility as a function of probe frequency relative to atomic resonance with EIT conditions (solid line) and without EIT conditions (dashed line). Note that under the EIT regime, absorption rapidly drops at resonant frequency [4].

1.2.2   Four-Wave Mixing

The FWM process occurs with the same set of hyperfine atomic levels used in EIT, this time arranged in a double-Λ configuration (figure 4). As with EIT, a control field and a probe field are each tuned from one ground state to an excited state. However, in reality, they are slightly detuned from their respective transitions, where the difference in frequency, the two-photon detuning (Δ), between the control and probe fields is equal to the difference between ground levels:

$$\Delta \equiv \omega_c - \omega_p. \tag{5}$$

Theoretically, the FWM effect emerges from the electric susceptibility. Its origin has been fully developed [5], and only a brief summary will be described in this paper. The total electric field can be expressed as the sum of the control and probe fields:

$$\mathbf{E} = E_{o_c} cos(\mathbf{k_c} \cdot \mathbf{r} - \omega_c t) + E_{o_p} cos(\mathbf{k_p} \cdot \mathbf{r} - \omega_p t) \tag{6}$$

where the subscripts c and p refer to the control and probe fields, respectively. The third order term of electric susceptibility describes a new electric field, conjugate with the probe field, which propagates in a direction $\mathbf{k_s} = 2\mathbf{k} - \mathbf{k_p}$ and has a frequency of $\omega_s = 2\omega_c - \omega_p$ to satisfy momentum conservation [6]. This third field, referred to as the Stokes field, couples with the strong control

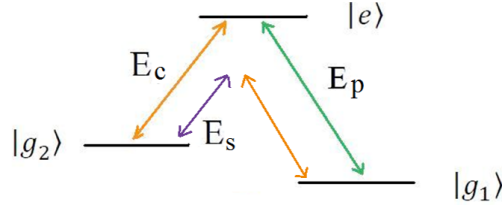field at specific laser detunings and becomes entangled with the probe field.

Figure 4: Double Λ regime for FWM.

2   Methodology

A Ti-Sapph laser was used for our control and probe fields. For our purposes, the control field was tuned to a frequency ν_0 around the F = 2 to F' = 2 transition and an orthogonally polarized probe field was tuned around the F = 2 to F' = 1 transition. To achieve a two-photon detuning close to resonance, the probe beam was sent through an electro-optic modulator, and the higher frequency sideband with a modulation frequency ν_m near to the hyperfine splitting of Rb ground states, 6.8 GHz, was filtered out using a Fabry-Peròt etalon (figure 5).
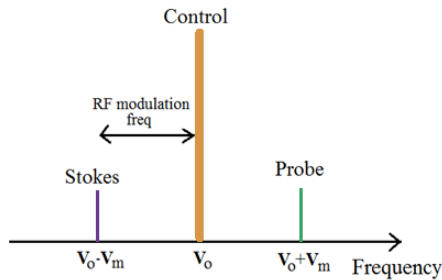

Figure 5: Three fields sent into Rb cell after EOM. Lines are representative of the relative intensities.

Figure 6: Sample Rb vapor cell.

The control and probe beams were then recombined using a polarizing beam splitter and sent into the Rb cell. The Rb cell used was 6 cm in length, magnetically shielded, and heated to 88°C. The high temperature allows for a larger atomic density within the the cell, which pronounces the EIT and FWM effects. The two beams were also adjusted to have a slight crossover angle, ($\theta \approx 0.5^{o}$). Because the Stokes field propagates in a direction $\mathbf{k_s} = 2\mathbf{k} - \mathbf{k_p}$, and therefore makes an angle equal but opposite to the probe field, with respect to the control field (figure 8). Other

experiments report FWM produced under crossover angles around our value, but always with $\theta < 1^o$ so as to create enough spatial overlap between the beams within the cell [7, 8, 9]. Lenses were also used to collimate, and increase the intensity of the beams within the cell. A diagram of the experimental setup is shown in figure 13.
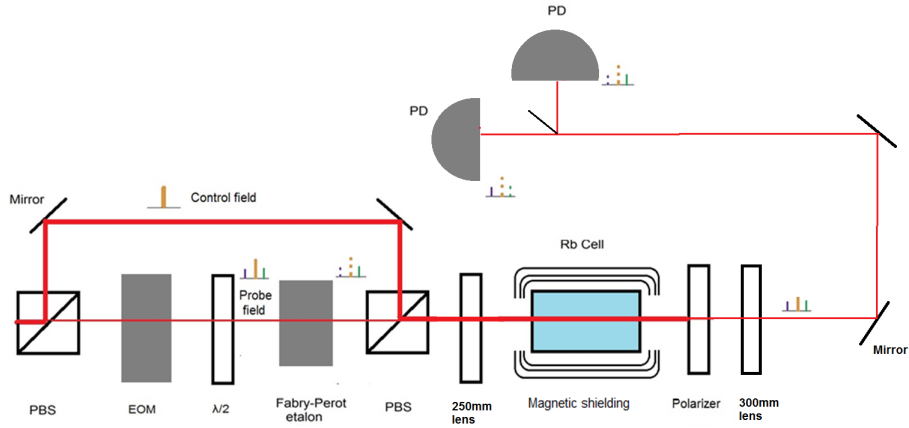

Figure 7: Diagram of experimental setup.

After the cell, the beams were spatially separated using an edge mirror so that the probe beam could be directed to one photodetector and the Stokes signal to another.
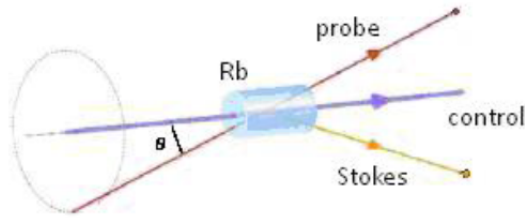

Figure 8: Exaggerated diagram of conjugate propagation directions between probe and Stokes fields under FWM conditions.

3   Results

3.1   Amplitude Characterization

Due to the slight crossover angle, the probe and control beams could be clearly resolved after the Rb cell, and photographs were taken of the fields. The intensity of the control beam was maximally reduced with a polarizer in order to improve resolution of the probe and Stokes fields. Under EIT and FWM conditions, a Stokes field was produced (figure 9b). The probe beam also experienced amplification as a result of the interaction within the cell.

(a) Laser beams with frequencies detuned far off resonance, away from EIT and FWM conditions. $\omega_c = 6.8341$GHz.

(b) Detuned to resonance, at EIT and FWM conditions. Stokes field becomes apparent. $\omega_c = 6.8351$GHz.
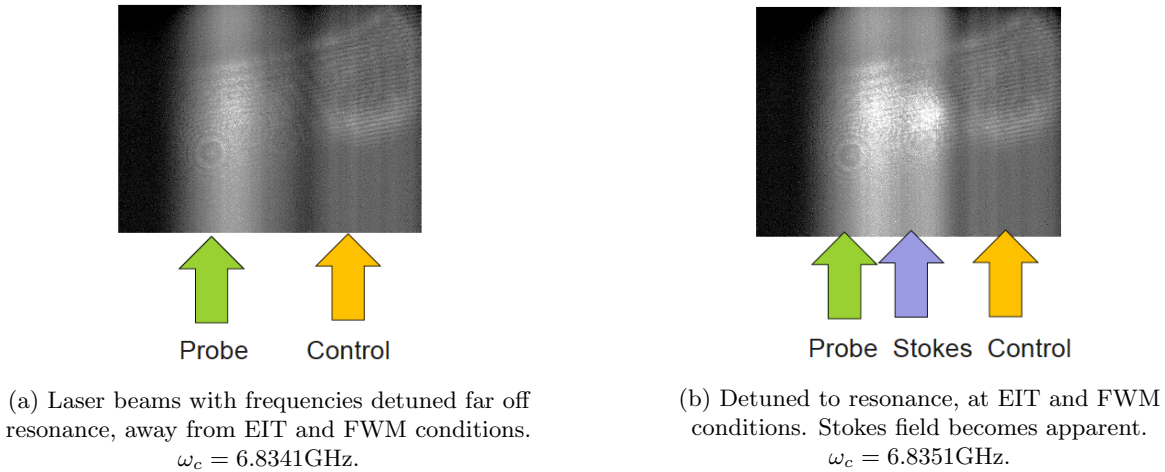
Figure 9: Photographs of electric fields after Rb cell.

The amplitude dependence of EIT and FWM lineshapes on laser power and detuning were investigated. Figures 10a and 10b show an example of the variation in EIT and FWM lineshapes due to laser detuning. The highest gain that the probe and Stokes fields experienced occurred at 794.9805 nm which is -0.004827 nm from the F $= 2$ to F' $= 1$ transition (figures 10c and 10d). Amplitude dependence on laser power is also shown (figure 11).
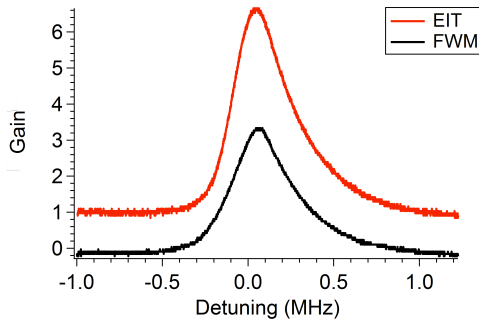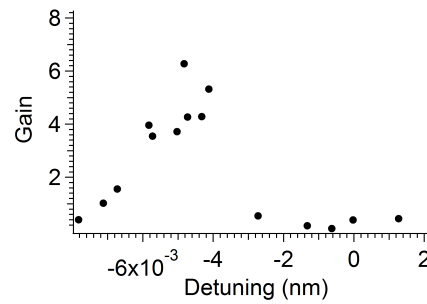
(a) EIT and FWM signals at 794.9801 nm.
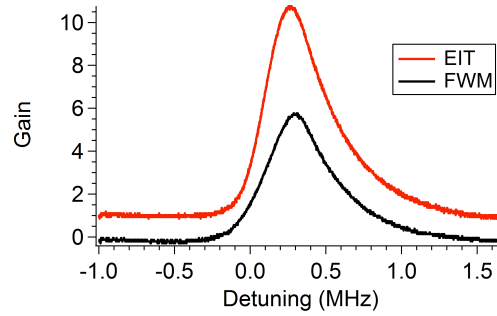
(b) EIT and FWM signals at 794.9809 nm.
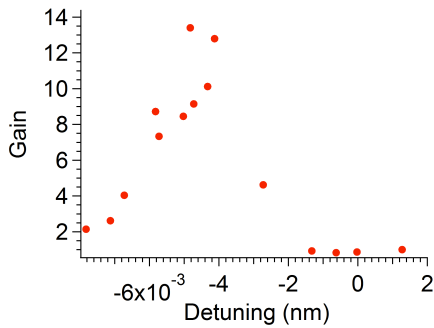
(c) Dependence of EIT amplitude on laser detuning. Amplitude measurements taken relative to off resonance probe signal and detunings measured from the $F = 2$ to $F' = 1$ transition.

(d) Dependence of FWM amplitude on laser detuning. Amplitude measurements taken relative to off resonance probe signal and detunings measured from the $F = 2$ to $F' = 1$ transition.
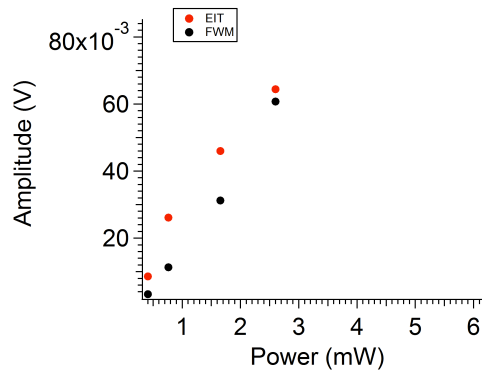
Figure 10

Figure 11: EIT and FWM amplitude dependence on laser power.

3.2 Correlation

As aforementioned, the key indicator of entanglement is the correlation that occurs between systems. The probe and Stokes signals were measured and analyzed to extract the correlation between the two fields. The function describing the correlation between intensities of the two optical fields is given by [10]:

$$G(\tau) = \frac{\langle \delta I_1(t)\, \delta I_2(t + \tau)\rangle}{\sqrt{\langle [\delta I_1(t)]^2\rangle\, \langle [\delta I_2(t + \tau)]^2\rangle}}. \tag{7}$$

Here, averaging the signals over time is defined as $\langle Q(t)\rangle = \int_t^{t+T} Q(t)/T\ dt$. Where T is the time of integration, in this report $T = $ [insert integration time], and τ is the time delay between signals. For our calculations we were exclusively interested in the correlation at $\tau = 0$.

[more data goes here]

4 Discussion

[discussion of FWM, correlation results]

5 Paraffin Coated Rb Cell

FWM was generated in an uncoated Rb vapor cell. However, a paraffin coated Rb cell was investigated as a possible alternative. When the Rb atoms interact with the coherent laser field, they are prepared in a quantum state. In a simple vapor cell without anti-relaxation coating, the atoms become depolarized upon colliding with the cell walls, and their quantum state is destroyed. To preserve the quantum memory of the atoms, coating such as paraffin which has a low absorption energy for atoms, can reduce surface relaxation. Thus, the coating can enable atoms to retain their quantum state, sometimes up to 10,000 collisions before depolarization occurs [11]. The effect of the paraffin coating was investigated to see whether this would enhance the EIT and FWM effects.

Due to the paraffin coating, there are two timescales where relevant effects occur. One timescale is on the the kHz range, and is a product of atoms which pass through the beam region in the cell only once (Figure 15a). The laser field prepares their quantum state for the time they interact with the light which results in a very short interaction time, t_{int}, but a wider feature in the frequency domain. The second timescale occurs in the Hz range, and is due to the paraffin coating. Because paraffin coating allows atoms to retain their quantum state even after collisions with the cell walls, it is possible for the atoms to interact with the laser beam several times (Figure 15b). This results in a feature with a much longer t_{int}, and a much narrower spectral feature [2].
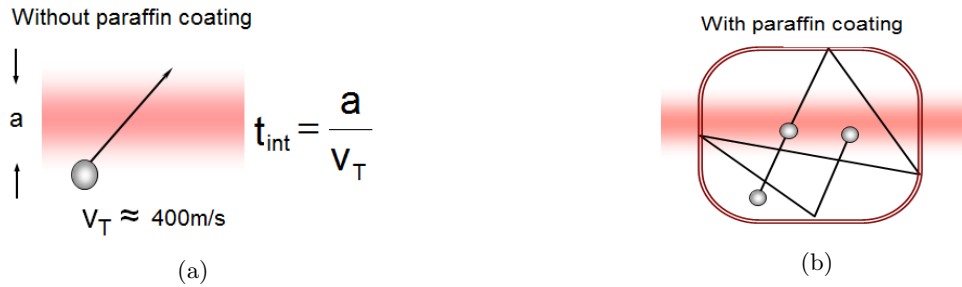

Figure 12: Simplified diagrams of atom interaction with light inside cell. Vapor cell has a diameter of about 5 cm.

To isolate the effect of the paraffin coating, the control and probe fields were spatially separated in our setup in an effort to enhance any narrow feature. The weak beam was split off at 10% of the power from the full laser beam and its transmission was analyzed with the photodiode (Figure 13). The main beam could then either co-propagate with the weak beam in the Rb cell or be stopped before the cell with the use of an iris.
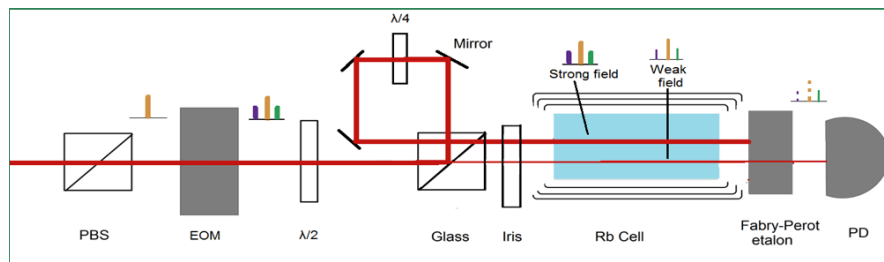

Figure 13: Experimental setup to investigate paraffin coating.

Each beam was composed of the three electric fields: probe, control, and Stokes fields. Alone,

the weak beam was not powerful enough to interact with the atoms in an observable manner on the narrow feature timescale; the populations that occupy the quantum states needed for EIT and FWM were too small to see. However, if the large beam was allowed to propagate inside the Rb cell in a different spatial region than the weak beam, it was powerful enough to prepare atoms in the relevant quantum states. Some of these atoms would then travel from the large beam region to the weak beam region. EIT and FWM features subsequently appeared in the weak beam's transmission signal. We expected that this change could be attributed primarily to the paraffin coating, as the vast majority of atoms that travel through the large beam would have to bounce against the cell walls multiple times before entering the region of the weak beam.

The RF modulation ramp was decreased from $6.8\,\mathrm{MHz}$ to $0.5\,\mathrm{MHz}$ in order to search for narrow spectral features. When the weak beam alone was sent through the cell, there was no evidence of a narrow feature. When the strong beam was sent co-propagating with the weak beam through the cell, a narrow feature did become observable.

(a) EIT with only weak beam, no evidence of a narrow feature on smaller timescale.

(b) EIT with both strong and weak beam, narrow feature apparent at smaller timescale.

(c) FWM with only weak beam, no evidence of a narrow feature on smaller timescale.

(d) FWM with both strong and weak beam, narrow feature observable at smaller timescale.
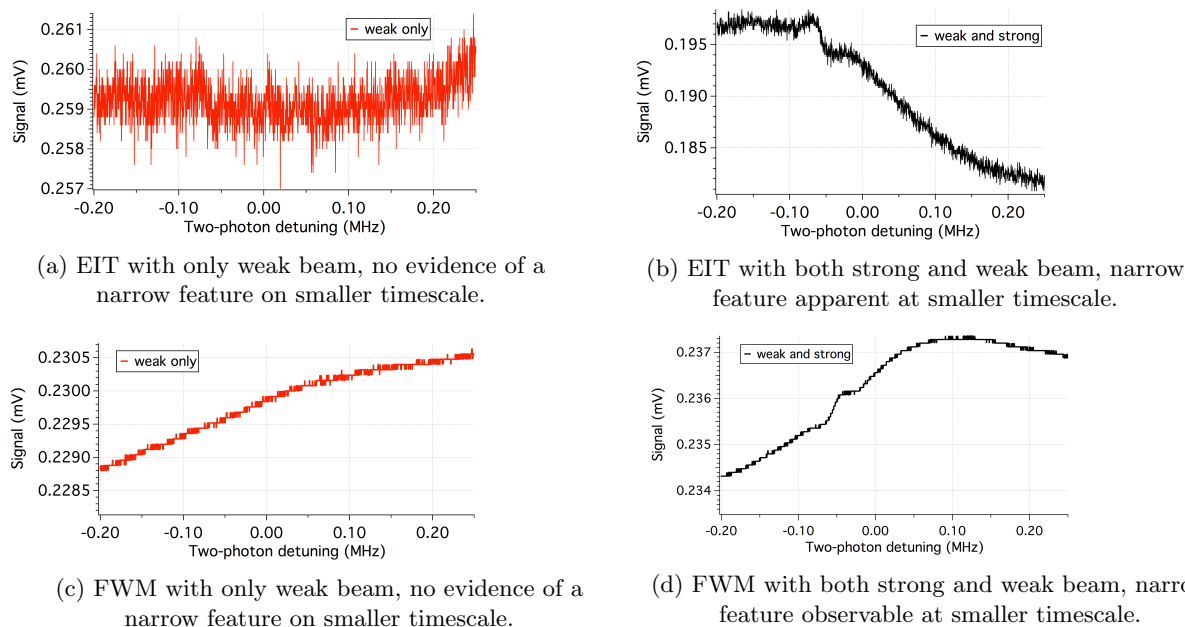
Figure 14: (a), (b) were observed on the EIT, probe, sideband while (c), (d) were observed on the FWM, Stokes sideband.

Although a narrow feature was observable, it was not as narrow as expected. The paraffin coated cell had first been tested under the Zeeman effect, to ensure that the paraffin coating produced

two timescales of spectral features. In the presence of a magnetic field a splitting of spectral lines occurs which causes an easily observable gain (much more so than EIT and FWM effects) in the light signal about resonant frequencies. With the paraffin coated cell, the narrow feature for the Zeeman effect was was three orders of magnitude narrower than the broad feature. But the EIT and FWM feature widths differed by, at most, only one order of magnitude. To investigate the suspicious width of the narrower feature, the paraffin-coated cell was switched out for an uncoated cell. The uncoated cell was found to have the same narrow feature, clearly demonstrating that it could not be an effect of the paraffin coating.

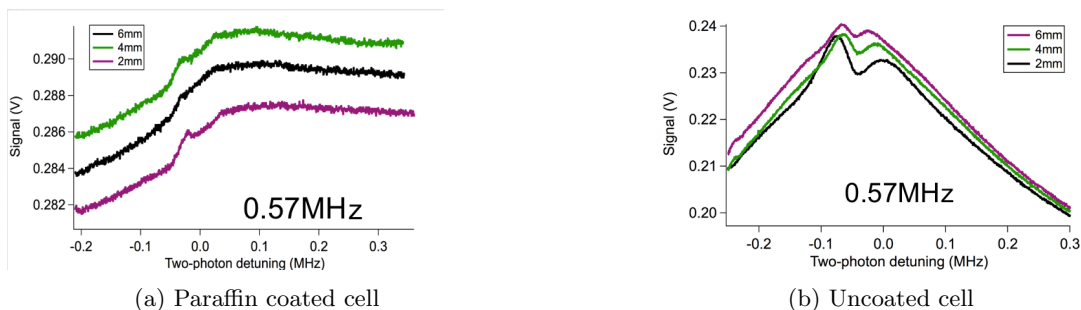(a) Paraffin coated cell   (b) Uncoated cell

Figure 15

Instead, the narrower feature was found to be dependent on spacing between the strong and weak beams. The amplitude of the feature increased as the distance between beams decreased. Therefore, rather than being an effect from the paraffin coating, the observed narrower feature was actually a result of atoms passing directly from one beam to the other. We suspect the effect of the paraffin coating was unobservable due to the time dependent phase of the bright and dark states (which differ from each other only by a sign). The dark state, which is rewritten from an earlier equation:

$$|B, D\rangle = E_c e^{ik_c z} |g_1\rangle \pm E_p e^{ik_p z} |g_2\rangle \tag{8}$$

$$|D\rangle = E_c |g_1\rangle - E_p e^{ik_p z - ik_c z} |g_2\rangle \tag{9}$$

It was calculated that an atom travels a transverse distance on the order of $1\,\mathrm{cm}$ before experiencing a phase shift of π, which turns its dark state into a bright state. It should be noted that our cell is on the order of $5\,\mathrm{cm}$, and that there is a high probability that the atoms travel more than $1\,\mathrm{cm}$,

especially with the use of paraffin coating. Therefore, the paraffin coating had no observable effect in the EIT and FWM regimes.

6   Conclusion

In conclusion, by sending two phase modulated laser beams through a Rb vapor cell heated to 88°C, we were able to produce EIT. FWM was also present within the cell which generated a third, Stokes, optical field that was identified by spatial angle. We investigated the probe and Stokes fields' dependence on laser detuning and power. For our specific setup, we found that the optimal EIT and FWM conditions, the conditions where the signals experienced the highest gain, were at a frequency of 794.9805 nm. We also measured correlation between the probe and Stokes fields.

As a potential method to increase atomic lifetimes and enhance EIT and FWM effects, we also investigated the use of paraffin coating on the Rb cell walls. A narrow spectral feature was identified, however it became apparent that the feature was a result of atoms flying directly between the spatially separated control and probe beams. Thus, we determined that the paraffin coating has an unobservable, and inconclusive, effect on EIT and FWM.

7   Acknowledgements

8   References

1. Einstein, A., Podolsky, B., Rosen, N. "Can Quantum-Mechanical Description of Physical Reality Be Considered Complete?" PR **47**, 777 (1935). doi: 10.1103/PhysRev.47.777.

2. Raimond, J. M., Brune, M., Haroche, S. "Manipulating Quantum Entanglement with Atoms and Photons in a Cavity." Rev. Mod. Phys. **73**, 565 (2001). doi: 10.1103/RevModPhys.73.565.

3. M. Klein, M. Hohensee, A. Nemiroski, Y. Xiao, D.F. Phillips, R.L. Walsworth. "Slow light in narrow paraffin-coated vapor cells." APL **95**, 091102 (2009).

4. Fleischhauer, M., Imamoglu, A., Marangos, J. "Electromagnetically Induced Transparency: Optics in Coherent Media." Rev. Mod. Phys. **77**, 633 (2005). doi: 10.1103/RevModPhys.77.633.

5. P. R. Berman, X. Xu. "Four-wave mixing in a Λ system." PRA **78**, 053407 (2008).

6. F. Fornasini. "The application of four-wave mixing to cold and ultra-cold atom imaging." Senior Thesis, The College of William and Mary (2010).

7. Pooser, R. C., Marino, A. M., Boyer, V., Jones, K. M., Lett, P. D. "Quantum Correlated Light Beams from Non-Degenerate Four-Wave Mixing in an Atomic Vapor: the D1 and D2 Lines of ^{85}Rb and ^{87}Rb." Optics Express **17**, 19 (2009). doi: 10.1364/OE.17.016722.

8. Boyer, V., Marino, A. M., Pooser, R. C., Lett, P. D. "Entangling Light in its Spatial Degrees of Freedom with Four-Wave Mixing in an Atomic Vapor." ChemPhysChem **10**, 5 (2009). doi: 10.1002/cphc.200800734.

9. Boyer, V., McCormick, C. F., Arimondo, E., Lett, P. D. "Ultraslow Propagation of Matched Pulses by Four-Wave Mixing in an Atomic Vapor." PRL **99**, 143601 (2007). doi: 10.1103/PhysRevLett.99.143601.

10. Sautenkov, V., Rostovtsev, Y., Scully, M. "From EIT Photon Correlations to Raman Anti-Correlations in Coherently Prepared Rb Vapor." PRA **72**, 065801 (2005), doi: 10.1103/PhysRevA.72.065801.

11. Budker, D., Romalis, M. "Optical Magnetometry." Nature Physics **3**, 227-234 (2007). doi: 10.1038/nphys566.